Society For Biomaterials

Synthesis and characterization of a novel scaffold for bone tissue engineering based on Wharton's jelly

Cristian Martínez,[1,2,3] Carlos Fernández,[1] Miguel Prado,[4] Andres Ozols,[1] Daniel G. Olmedo[2,5]

[1]Department of Oral Pathology, Group of Biomaterials for Prostheses, Institute of Biomedical Engineering, Engineering School, Buenos Aires University,
Av. Paseo Colón 850 (C1063ACV), Argentina
[2]Laboratory for the Study of Biomaterials, Department of Oral Pathology, School of Dentistry, University of Buenos Aires, MT de Alvear 2142, 2° "A", (C1122AAH), Argentina
[3]Biomaterials Group, School of Dentistry, National University of Cuyo, Mendoza, General San Martin Park (M5502JMA), Argentina
[4]Nuclear Materials Group, Bariloche Atomic Center (GMN-CAB), National Atomic Energy Commission, Av. E. Bustillo 9500, San Carlos de Bariloche, (R8402AGP), Argentina
[5]National Research Council (CONICET), Buenos Aires (C1122AAH), Argentina

Received 6 July 2016; revised 10 November 2016; accepted 6 December 2016
Published online 2 February 2017 in Wiley Online Library (wileyonlinelibrary.com). DOI: 10.1002/jbm.a.35976

Abstract: A composite is a material made of more than one component, and the bond between the components is on a scale larger than the atomic scale. The objective of the present study was to synthesize and perform the structural characterization and biological evaluation of a new biocomposite (BCO) based on a novel combination of an organic and an inorganic phase, for bone tissue engineering applications. The organic phase consisted of Wharton's jelly (WJ), which was obtained from embryonic tissue following a protocol developed by our laboratory. The inorganic phase consisted of bioceramic particles (BC), produced by sintering hydroxyapatite (HA) with β- tricalcium phosphate (β-TCP), and bioactive glass particles (BG). Each phase of the BCO was fully characterized by SEM, EDS, XRD, and FTIR. Biocompatibility was evaluated *in vivo* in the tibiae of Wistar rats ($n = 40$). Histological evaluation was performed at 0, 1, 7, 14, 30, and 60 days. XRD showed the phases corresponding to HA and β-TCP, whereas diffractogram of BG showed it to have an amorphous structure. EDS showed mainly Si and Na, Ca, P in BG, and Ca and P in HA and β-TCP. FTIR identified bonds between the organic and inorganic phases. From a mechanical viewpoint, the composite showed high flexural strength of 40.3 ± 0.8 MPa. The synthesized BCO exhibited adequate biocompatibility as shown by formation of lamellar type bone linked by BG and BC particles. The biomaterial presented here showed excellent mechanical and biocompatibility properties for its potential clinical use. © 2017 Wiley Periodicals, Inc. J Biomed Mater Res Part A: 105A: 1034–1045, 2017.

Key Words: biocomposite, biomaterial, Wharton's jelly, bone regeneration, biomimetic material

How to cite this article: Martínez C, Fernández F, Prado M, Ozols A, Olmedo DG. 2017. Synthesis and characterization of a novel scaffold for bone tissue engineering based on Wharton's jelly. J Biomed Mater Res Part A 2017:105A:1034–1045.

INTRODUCTION

Bone tissue can be injured in a variety of clinical situations (cysts, tumors, trauma or hormonal diseases) generating bone defects, which can be repaired by the body.[1] However, when the defect exceeds a certain critical size, the repair process is affected, and bone tissue engineering is necessary.[2,3] Bone tissue engineering is based on three pillars: the use of three-dimensional scaffolds, biomolecular signals, and cells. The ultimate goal of bone tissue engineering is to develop bony tissues on tissue engineered constructs that mimic the native bone. Scaffolds are the basis of bone tissue engineering (BTE), and are designed to interact with body tissues to produce a specific response and provide an ideal environment for bone formation. They must allow cell adhesion and proliferation, be replaced by the host tissue, have adequate mechanical behavior, and produce no immune response in the patient.[2–4] Seventy percent of bone consists of minerals and 30% is organic material.[5] The inorganic phase consists of hydroxyapatite (**HA**) $[Ca_{10}(PO_4)_6(OH)_2]$, a calcium phosphate salt, which provides bone with hardness and strength, whereas the organic phase mainly consists of type I collagen, which provides tensile and flexural strength.

At present, most research on the synthesis of scaffolds focuses on the use of composite materials known as biocomposites **(BCO)**, which consist of an organic and an inorganic phase in order to mimic the bone tissue structure

Correspondence to: Cristian Martínez; e-mail: yo.cristian.martinez@gmail.com
Contract grant sponsor: UBACyT (University of Buenos Aires, Argentina); contract grant number: 20020150100032BA and 0020130100332BA
Contract grant sponsor: PIP (National Council for Scientific and Technological Research, Argentina); contract grant number: 11220130100091

(biomimetic concept).[6] Such scaffolds not only mimic the extracellular matrix of bone, but also combine the inherent intrinsic advantages while minimizing the drawbacks of each phase. The organic phase can consist of natural or synthetic polymers. It must be pointed out, however, that polymers have poor mechanical performance in practical clinical applications. Natural polymers such as polysaccharides (alginate, chitosan, or various cellulose compounds) and protein (collagen, silk) are most commonly used today.[7–9]

The use of Wharton's jelly (**WJ**) as the organic phase would enhance the regenerative capacity of the tissue.[10] WJ consists mostly of collagen, glycosaminoglycans (GAGs) (mainly hyaluronic acid and chondroitin sulfate) and growth factors, providing a temporary anchorage for the three-dimensional adhesion, proliferation and differentiation of cells. WJ forms a hydrogel that provides a suitable platform for intercellular communication, matrix–cell–biomaterial interactions, and secretion of signaling molecules, which are responsible for directing the regenerative process.[10]

The most frequently used components for the inorganic phase are bioceramic (**BC**) and bioactive glass particles (**BG**), both of which are known for their osteoconductive properties. The degradation rate of BC matches the growth rate of the target tissue.[11–13] As regards BG, this biomaterial has the ability to form HA on its surface, forming chemical bonding with the bone tissue, and to stimulate certain genes, increasing the population of osteoblasts at the bone defect site.[12–16] The rationale for combining both biomaterials was that silica–calcium phosphate-based compounds have a pro-osteogenic effect on bone cells, improving cell attachment and proliferation.[17] The release of calcium, phosphorus, and silica ions into the biological environment generates an increase in mRNA expression of osteocalcin and osteopontin in osteoblastic cells, and produces a significant increase in alkaline phosphatase activity.[18] Silica, in turn, plays an important role in bone marrow cell differentiation, increasing the phenotypic expression of osteoblasts.[19] In addition, it has been demonstrated that this type of implant coating induces higher protein adsorption, enhancing bone integration while minimizing the induction of inflammatory responses.[20]

The aforementioned issues prompted the present work, in which a novel use of WJ as a three-dimensional matrix in combination with BC (HA and β- tricalcium phosphate, β-TCP) and BG particles, is proposed. This kind of combination would generate a synergistic effect resulting in a bone-like tissue, enhancing the biological and mechanical behavior of BCO.

The objective of this work was to synthesize and perform the structural characterization and biological evaluation of a new WJ-BC-BG-based biocomposite for bone tissue engineering, which has the ability to facilitate bone tissue regeneration.

MATERIALS AND METHODS

The BCO presented herein is made of BC (HA + β-TCP) and BG particles as the inorganic phase, and of WJ acting as a three-dimensional organic matrix (Fig. 1).

Obtaining the biocomposite (BCO)

Synthesis of the bioceramic (BC). HA was obtained from bovine bone, in keeping with the current rules and regulations of the Argentine national agricultural health service (SENASA) and in compliance with traceability regulations, using specific methods for inactivation and removal of infectious agents (Committee for Proprietary Veterinary and Medicinal Products), and removal of bone marrow, blood and fat. The bone was cut into 5–20 cm^3 pieces. To remove hemoglobin and adipose tissue, 10 kg of bone were placed in 20-L buckets and washed six times by successive immersion for 48 h in aqueous solutions of ammonium bicarbonate (0.2% in wt.), sodium hydroxide (0.2% in wt.), hydrogen peroxide (0.3% in wt.), and glacial acetic acid (100% in wt. of bone), using fresh solutions each time; the solutions were maintained at a constant temperature between 55 and 60°C using an electric immersion heater.

The degreased and blood-free bone was dried under forced hot air flow (using a centrifugal blower) inside a vertical metal muffle equipped with electric heaters. As a result, white spongy cortical bone was obtained. As shown by XRD analysis, it was composed only of HA. The obtained material was dry ground in a ball mill (in a 10-L porcelain pot, employing 1″ diameter AISI 420 hardened steel balls) for 5 h. The powder was sieved manually to separate the particle fraction of <45 μm in size (ASTM#325) in agreement with standard ISO 13779–6: 2015 (Implants for surgery–Hydroxyapatite–Part 6: Powders). The grains of β-TCP were synthesized by wet precipitation,[21] by addition of an acid solution of H_3PO_4 to a suspension of $Ca(OH)_2$ (Merck, Germany; both chemicals were of analytical grade) at pH 6 and 22°C, under constant agitation. The precipitate was composed mainly of calcium deficient HA, which was filtered, oven dried, and sintered at 1100°C for 2 h, in order to promote transformation into crystalline β-TCP. The presence of β-TCP phase and the degree of crystallinity were verified by X-ray diffraction (XRD), in agreement with standard ISO 13175–3: 2012 (Implants for surgery–Calcium phosphates–Part 3: Hydroxyapatite and beta-tricalcium phosphate bone substitute). The fractions smaller than 45 μm of β- TCP particles were also separated.

For blending, 480 g of HA powder, 60 g of beta-TCP powder, and 250 g of ethyl alcohol (95% v/v) were placed in 2-L liquid-tight PVC jars and mixed using 10 to 15 (¾- 1 inch) porcelain balls as the grinding medium. The jars were placed horizontally on the rollers and rotated at 150 rpm for 3 h. The obtained slurry and the balls were placed in stainless steel bowls and dried in an electric oven at 70°C for 3 h; the mixture was then placed in the jars and milled gently, and the balls were removed from the powder by hand. The obtained powder was dispersed in a 15% (in wt.) aqueous solution of egg albumin, in a 1: 1 solid//liquid ratio, which was homogenized by stirring at 300 r.p.m. for 10 min. The viscous fluid was cast into silicone rubber molds, which were wrapped in PVC film and subjected to heating at 90°C in a thermostatic bath for 1 h. The gelled pieces ($5 \times 10 \times 50$ mm^3) were oven dried and then placed in an electric furnace and heated at a rate of 10°C min^{-1} up

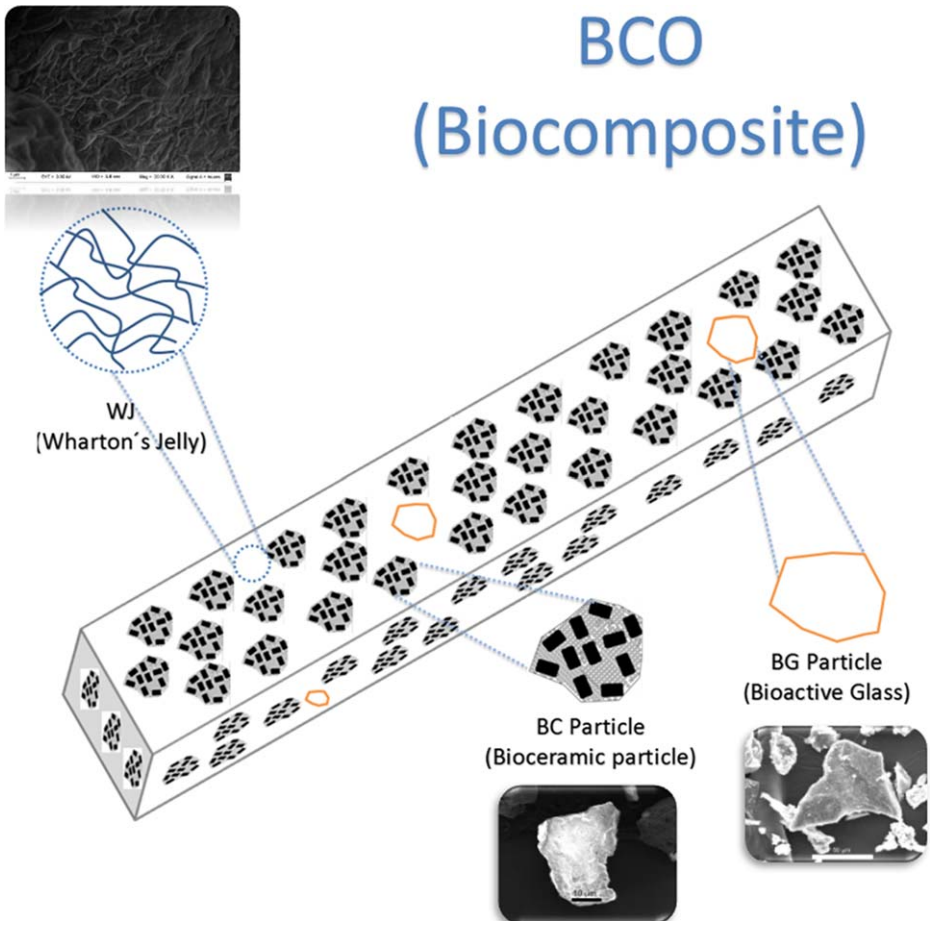

FIGURE 1. Schematic drawing of the Biocomposite and its components.

to a sintering temperature of 1200°C and maintained at that temperature for 2 h. Finally, the samples were cooled to room temperature at a slow rate. The product was ground and sieved to retain particles in the range of 150–350 μm.

Synthesis of bioactive glass (BG). BG was obtained by mixing 45 g of SiO_2, 43.32 g of $CaCO_3$, 38.01 g of Na_2CO_3, 30.27 g of $Na_2HPO_4.2H_2O$ powders (Anedra, Argentine; all were analytical grade compounds) in a ball mill. This formulation was chosen to obtain a composition similar to 45S5 Bioglass^{TM}, as confirmed by atomic absorption analysis. The mixture was subjected to a thermal cycle in an electric furnace in air employing a 500 cm^3 Pt crucible. The cycle consisted of heating at 10°C min^{-1} up to 1350°C (well above glass melting point, which is close to 890°C), and maintaining the mixture at that temperature for 2 h. The molten material was cast onto a steel plate to produce rapid quenching. This process was repeated twice in order to guarantee composition homogeneity. BG particles were obtained by crushing and grinding a block of BG, and sieving to retain the 150–350 μm size fraction.

Obtaining the biological matrix from Wharton's jelly (WJ). The matrix was extracted by processing Human Wharton's jelly following a proprietary method, currently at the stage of patent preparation, which involves a number of physicochemical steps. The placentas and umbilical cords were provided by the department of Gynaecology and Obstetrics of Prof. Dr. Ramón Carrillo Hospital for Acute Diseases, (Buenos Aires, Argentina) in keeping with a protocol approved by the Research Ethics Committee (N° 1339).

Umbilical cords (∼20 cm) were collected from seven patients at full term delivery, placed in transport medium (Hank's Balanced Salt Solution supplemented with antimycotic—antibiotic solution, Invitrogen Life Technologies, CA), stored at 4°C, and processed within 12 h after collection. Each cord was cut into 2-cm long pieces, washed well in distilled water to remove blood and debris, and gently teased to squeeze out any trapped blood inside the veins and arteries. Each piece was cut open lengthwise with sterile scissors, and placed with its inner surface facing down in a 60 mm Petri dish in order to extract WJ. The material was subjected to several chemical processes (which will be described in the future patent), preserving the neutrality of the obtained WJ water solution. Finally, the solution was granulated in a spray dryer and maintained below 42°C. The entire process was conducted in a sterile area of a pharmacological laboratory, following a strict microbiological protocol to avoid contamination with pyrogens. WJ was sterile-packaged and stored in vacuum until use.

Obtaining the biocomposite. The inorganic phase was a mixture of 20 g of BG (5% of total weight) and 400 g of BC (95% of total weight). The organic phase was obtained by dissolving WJ granules in bi-distilled water at 10% (in wt.) at 25°C under constant stirring. The BCO were obtained by dispersion of inorganic particles in WJ solution in a 1:3 ratio (in wt%). To perform mechanical tests and to prepare the micro implants, the viscous fluid was injected into rubber molds with $5 \times 10 \times 50$ mm^3 wells using a 60-cm^3 glass syringe without needle in order to prevent the dispersed particles from obstructing the flow. CO dehydration was performed under a forced flow of sterile filtered air in a 4″ diameter glass tube for 48 h, in order to obtain stiff pieces that would not lose their shape. The pieces were wrapped in surgical article and polyethylene bags, and sterilized by gamma irradiation at a dose of 10 kGy.

The stiffness of BCO pieces was suitable for cutting with a manual saw to obtain $5 \times 10 \times 50$ mm^3 samples for the mechanical tests. Laminar implants measuring $6.0 \times 1.0 \times 1.0$ mm^3 were obtained to assess biological response.

Structural, mechanical, and biochemical characterization

The microstructure of the BC, the BG and BCO was analyzed by scanning electron microscopy (SEM, Zeiss Supra model 40, Germany), and local chemical analysis was performed by Energy- dispersive X-ray spectroscopy (EDS, Oxford Instruments, UK). Identification of the crystalline phases was performed by X-ray diffraction (XRD, Rigaku, Japan) using Cu Kα radiation (λCu Kα = 0.1542 nm) with Ni filter, in a vertical goniometer, with 2θ scanning angle range of 20–70° and a step size of 0.2°. The chemical nature of bonds was studied by infrared Fourier transform spectroscopy (FTIR, Perkin-Elmer, model Frontier®, USA) in Attenuated Total Reflectance (ATR) mode, registering at 4 cm^{-1} resolution averaging 50 scans over a range of wavenumbers 400 cm^{-1} to 4000 cm^{-1}.

Mechanical strength was assessed by using a three-point bending test on 20 BCO samples measuring $5 \times 10 \times 50$ mm^3. The measurements were made in a universal testing machine (Instron 5960, USA) under a load of 500 N and at a crosshead speed of 1 mm min^{-1}, until fracture following plastic deformation. Flexural strength, σ_f (in MPa), was determined using the following equation:

$$\sigma_f = 3\ FL/2bd^2$$

F is the load at a given point on the load deflection curve, (N) L is the support span, 25 (mm), b is the width of test beam (in mm), and d is the depth or thickness of tested beam, (mm).

The flexural modulus, E_f, was calculated as follows:

$$E_f = \mathrm{Lm}/4\mathrm{bd}^3 \quad (2)$$

m is the slope of the initial straight-line portion of the load deflection curve, (N/mm).

In vivo bioassays

Male Wistar rats ($n = 60$, mean body weight: 150 g) were used in order to study biological response to BCO. The animals were fed *ad libitum*. All animal procedures were performed in accordance with the guidelines of the National Institutes of Health (NIH Publication—Guide for the Care and Use of Laboratory Animals: Eighth Edition (2011) and the guidelines of the School of Dentistry, Buenos Aires University (Res (CD) 352/02 y Res (CD) 694/02) for the care and use of laboratory animals.

The animals were anesthetized intraperitoneally with a solution of 8 mg of ketamine chlorhydrate (Fort Dodge®, Argentine) and 1.28 mg of Xylazine (Bayer, Germany) per 100 mg of body weight. The skin of both tibiae was shaved prior to performing a 1.5 cm incision along the tibial crest. The subcutaneous tissue, muscles and ligament were dissected to expose the lateral external surface of the diaphyseal bone. A hole measuring 1.5 mm in diameter was made in the bone with an end-cutting bur, using manual rotating movements to avoid overheating and necrosis of the bone tissue. BCO implants ($6.0 \times 1.0 \times 1.0$ mm^3) were placed in the hematopoietic bone marrow compartment of both tibiae, parallel to their longest axis. A separate-stitch suture was performed. No antibiotic therapy was administered.[22]

The animals were euthanized in groups of 10 by an overdose of anesthetic at 0, 1, 7, 14, 30, and 60 days post-implantation. The tibiae were resected, fixed in 10% formalin solution, and radiographed. One group of samples was demineralized in 7% nitric acid (Anhedra, Argentina), embedded in paraffin, and stained with H-E. The remaining group was embedded in methyl-methacrylate. The samples were then sectioned using a diamond saw (EXAKT Apparatebau, Germany) and three slices were cut at ~500 μm, perpendicular to the longest axis of the tibiae, that is, through the middle of the implant bed and at two points equidistant from the middle. The cross-sections were ground using a grinding machine and finished manually with sandpaper. Sections about 70-μm thick were stained with 1% toluidine blue and mounted on glass slides and coverslipped for histological analysis. The samples were examined using conventional and polarized light microscopy.

Histomorphometric determinations were performed to assess the area of newly formed lamellar bone in contact with the particles of the biocomposite with respect to the total area (40×). Histomorphometric measures were determined on digitized images of histological sections obtained 30 and 60 days post- implantation of the biomaterial into the tibia of Wistar rats. The images were obtained using a light microscope (Axioskop 2 MOT, Carl Zeiss, Jena, Germany) at 40× magnification, and they were analyzed histomorphometrically using Image Pro Plus software (Version 6.0) (Mediacybernetics Rockville, USA). The results were compared using Student's *t* test. Values are expressed as mean and SD; statistical significance was set at $P < 0.05$. A set of sections was coated with a thin (20-nm) layer of silver in a vacuum evaporator, for SEM and EDS.

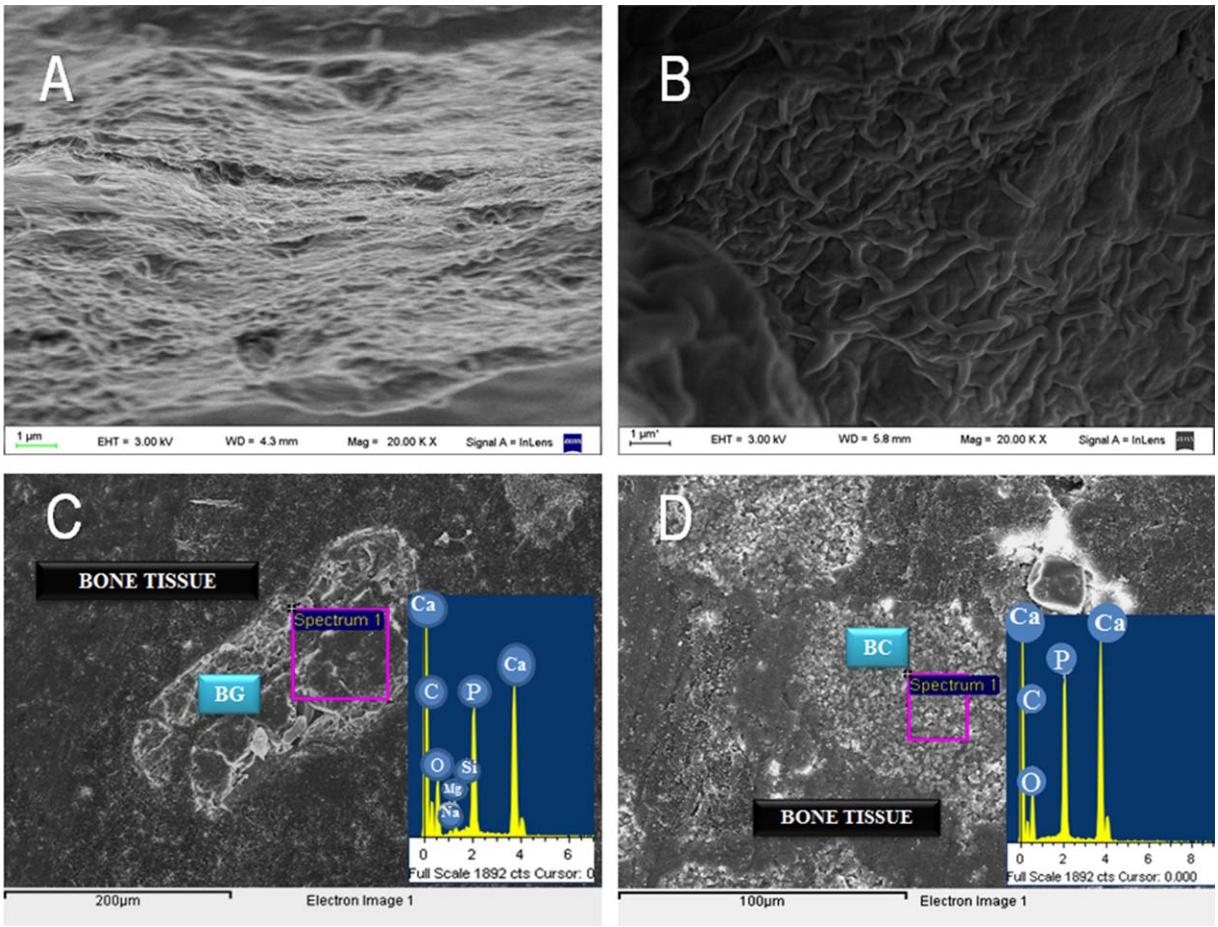

FIGURE 2. SEM images of the dehydrated biocomposite (BCO) (A), dehydrated Wharton Jelly (WJ) (B) and methyl-methacrylate histological sections (C, D); C and D also show microchemical analysis (EDS). (A) Uneven non-porous surface of the BCO. (B) Complex net-like structure of the dehydrated WJ. (C) Bone tissue around a BG particle. The spectrum shows the peaks corresponding to the main components of the BG (Si, Mg, Na and Ca). (D) Newly formed bone tissue in contact with the BC particles. The spectrum shows the peaks corresponding to the main components of the BC (Ca and P).

RESULTS

Structural, mechanical, and biochemical characterization

As shown by SEM, the surface of the BCO after molding and in a dehydrated state was uneven and non-porous [Fig. 2(A)] since the WJ covered the entire surface of the BCO during the manufacturing process. Higher magnification allowed observation of the fibrous structure of the WJ, with randomly arranged collagen bundles forming a complex net-like structure [Fig. 2(B)]. Analysis of cross sections of samples embedded in methyl-methacrylate observed by SEM showed BG and BC particles inside the newly formed bone [Fig. 2(C,D)].

EDS of histological sections showed mainly Si, Na, Ca, and P in BG, and Ca and P in HA and β-TCP [Fig. 2(C,D)]. SEM images and EDS spectra clearly showed the presence of BG in the BCO, even when the concentration of BG was low (5% of total weight) [Fig. 2(C)].

XRD analysis of the BC and BG confirmed their crystalline and amorphous nature respectively (Fig. 3). The BC was composed of HA (file 34–0010) and β-TCP (file 55–0898) phases. The BG, however, showed a single broad peak centered at 31.8° corresponding to SiO_2 (file 05–0492) [ICD05], with no evidence of other oxides, as shown by EDS and as observed in all bioactive glasses.[23,24]

Analysis of FTIR spectra of BC showed predominant presence of the PO_4^{3-} group in the 960–1109 cm^{-1} band, and 602, 565 and 475 cm^{-1}[25,26]; whereas the OH group was found in 3573 cm^{-1},[25–29] and 872 and 631 cm^{-1}.[29] In contrast, the spectrum of BG exhibited only a few peaks, which could be associated with the nominal composition of Bioglass™, despite the spectrum being rich in absorption peaks (Fig. 4). Vibrations of the PO_2 group could be observed at 1416 and 1445 cm^{-1}[1,30] and a small intensity peak of PO vibration could be observed at 595 cm^{-1}.[31] Vibrations associated with Si-O-Si amorphous silicate were detected at 1092 and 451 cm^{-1}.[30,31]

The biological matrix has amide functional groups, which are characteristic of collagen type I and II polypeptides (Fig. 4). Hence, amide I was present at 1656 and 1159 cm^{-1}[1,26–38] amide II was observed at 1539 cm^{-1},[35,36] amide III at 1452 and 1244 cm^{-1}[1,34–42] amide A at 3468 cm^{-1}[36,37] and amide B at 2968 cm^{-1}.[34–40] Other functional groups (CH_3, CH_2, CH) may have contributed to

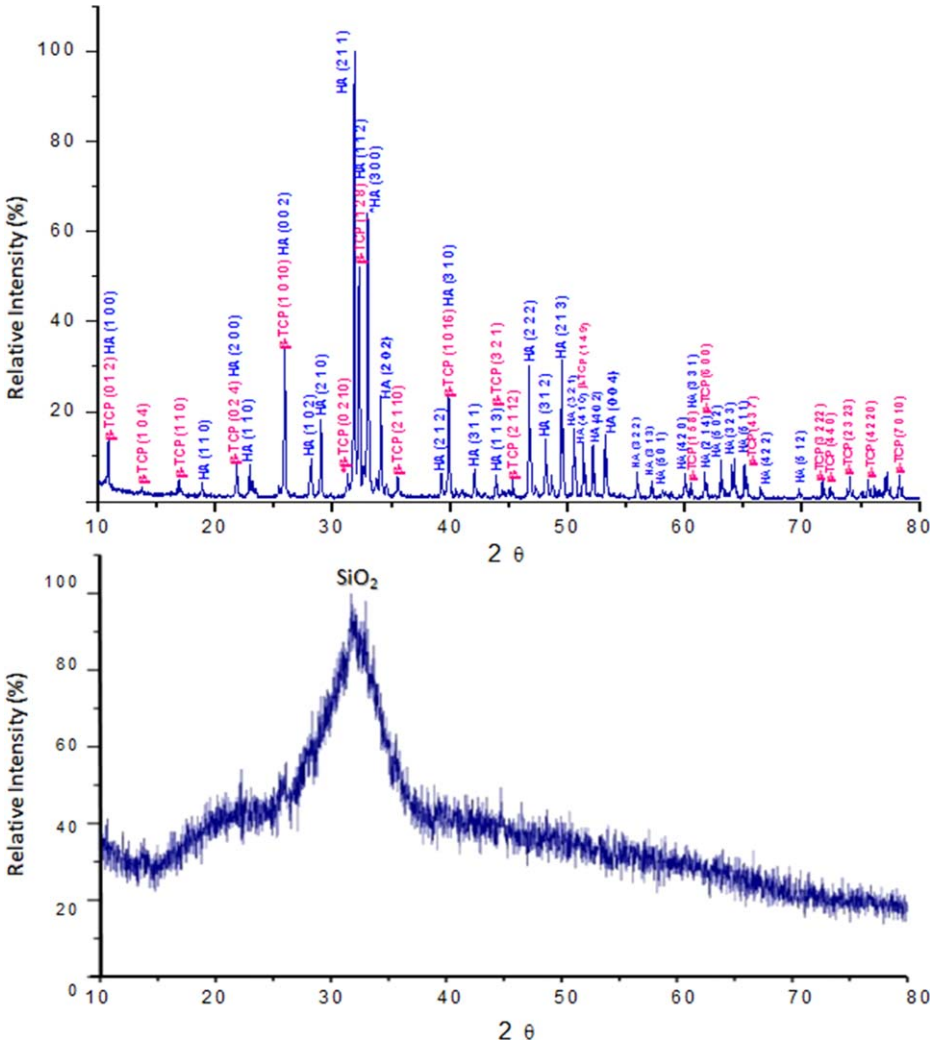

FIGURE 3. Diffractograms of BC (above) and BG (below).

absorption at 1339 cm^{-1}[42] (Fig. 4). The least clear association occurred at 1090 cm^{-1}, which may correspond to the vibrational states of C—C and C—N[38] Nevertheless, these results would not be sufficient to say that the matrix was collagen, and likely corresponds to isolated poly-peptide chains, resulting from the denaturation caused by the chemical treatments to which the WJ was subjected.

FTIR analysis of BCO showed overlapping of absorption peaks and bands of BC and biological matrix (WJ) phases, which were analyzed separately before BCO moulding (Fig. 4). The interaction between BC crystals and WJ, probably containing some amino acid residues of the poly-peptide chains, could be attributed to the phosphate band between 980 and 1150 cm^{-1},[34–42] whereas the 878 cm^{-1} could be attributed to the carbonation of HA, which closely resembles that of natural bone tissue[43] (Fig. 4). The presence of BG in the BCO was not discernible in FTIR and XRD, because of the low concentration of BG (5% weight of inorganic phase). However, BG particles could be detected on SEM images and by EDS analysis of histological sections [Fig. 2(C)]. In addition, SEM images showed partially resorbed BC particles [Fig. 2(D)].

Mechanical testing using the three point bending flexural test showed un-implanted dehydrated BCO blocks measuring 5 × 10 × 50 mm^3 to have a maximum flexural strength of (40.3 ± 0.8) MPa, whereas the flexural modulus was (2.44 ± 0.11) GPa.

Biological response

Paraffin embedded sections obtained at T_0 (immediately post-implantation) showed negative spaces corresponding to the inorganic particles in the BCO, which were amalgamated by large basophilic areas corresponding to the organic matrix of the biomaterial [Fig. 5(A,B)]. At 24 h post-implantation (T_{1d}), close contact between the BCO particles and the clot could be observed, evidencing the adequate wetting properties of the biomaterial. In addition, abundant polymorphonuclear neutrophils (PMNn) corresponding to the acute inflammatory infiltrate could be observed [Fig. 5(C,D)].

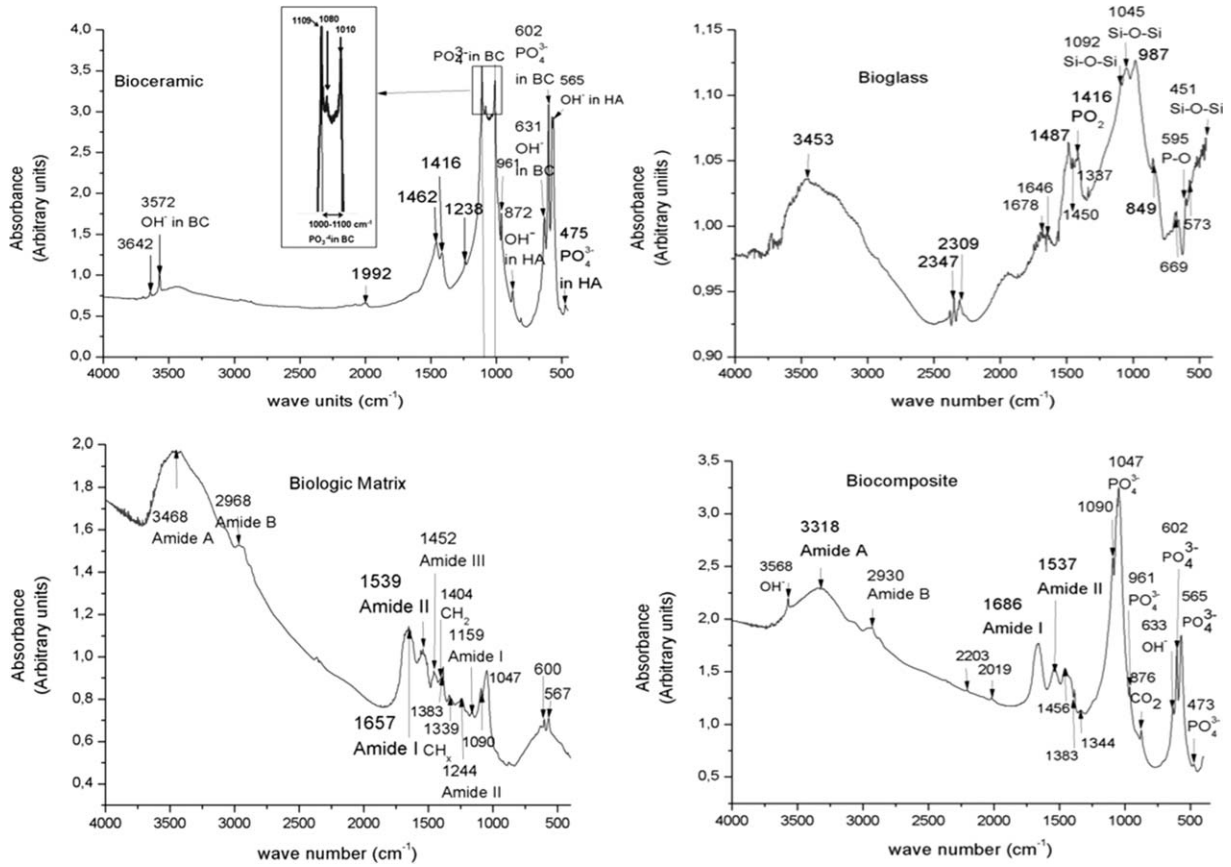

FIGURE 4. FTIR spectra of BC (top left), FTIR spectra of BG (top right), FTIR spectra of WJ (bottom left) and FTIR spectra of BCO (bottom right).

At 7 days post-implantation, formation of reparative granulation tissue with abundant fibroblasts in close contact with the BC and BG particles could be seen [Fig. 6(A–C)]. It is noteworthy that the organic matrix, made up of the WJ, was completely replaced with the reparative granulation tissue, and there was no evidence of inflammatory infiltrate at this time point. In addition, multinucleated giant cells could be seen at the center of the reparative tissue, but were not found at the later experimental times (Fig. 7). Fourteen days post-implantation, woven bone tissue (as confirmed by polarized light microscopy) could be observed amalgamating the BCO particles [Fig. 6(D–F)]. At 30 and 60 days, the woven bone had been replaced with lamellar bone (as confirmed by polarized light), which formed bridges of bone linking the BC and BG particles. The lamellar bone exhibited the typical microstructure with collagen fibers arranged in parallel lamellae or in concentric layers around canals containing vessels, forming the Haversian-systems. Osteocyte-containing lacunae were also observed between or inside the lamellae (Fig. 8).

The BCO particles and their interface with the bone tissue could be observed on the methyl-methacrylate embedded sections (image not shown).

The histomorphometric studies showed the area of lamellar bone to increase with time. The area of newly formed bone was $26.517{,}65 \pm 3.433{,}15$ μm^2 at 30 days (**T30)** and $48.638{,}23 \pm 3.736{,}77$ μm^2 at 60 days (**T60),** in a total area of 90.000 μm^2. The difference was statistically significant $P < 0.05$.

DISCUSSION

Bone can be considered a nano-composite material made up of collagen protein fibers threading through a HA mineral phase, which makes up about 60–70 wt % of the bone structure. Based on a biomimetic mechanism, we prepared a BCO with a biphasic organic/inorganic structure similar to that of natural bone.

The organic phase of the BCO was WJ. The latter mainly consists of various isoforms of collagen and proteoglycans, enabling it to form a hydrogel and serve as a reservoir of numerous growth factors including TGF-B, IGF-I, FGF, EGF, and PDGF.[44–46]

As shown by SEM, the WJ in the BCO consisted of collagen fibers forming a substantial three-dimensional net-like structure that was similar to that described by other authors,[47] and the BG and BC particles were intertwined with the fibers.

The wettability of BCO in a physiological environment is associated mainly with the presence of hydroxyl groups and negative charges in hyaluronic acid,[46] which is one of the components of WJ and is used in the synthesis of biological scaffolds for wound-healing applications. This property leads to rapid hydrogel formation and haemoglobin colonization in the scaffold, from the first moment after

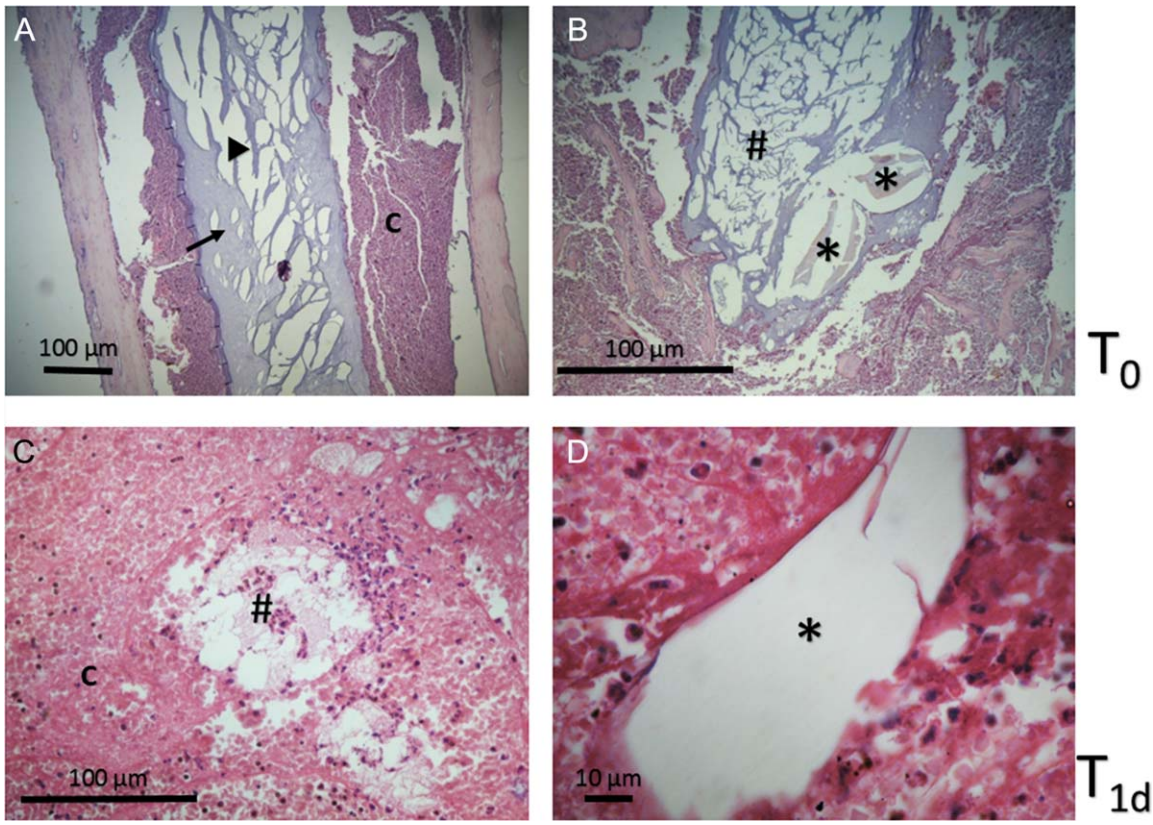

FIGURE 5. Histological study at T0 (A and B) and T1d (C and D). A) BCO inside the medullary compartment and surrounded by the blood clot (c); note the inorganic particles (▲) amalgamated by the organic matrix of the biomaterial (→). B) Bioactive glass (*) and BC particles (#) are surrounded by organic matrix. A) Orig Mag ×100. B) Orig. Mag. X400. H-E Stain. C) BC (#) surrounded by the blood clot (c). (D) Visualization of a BG particle (*) surrounded by the clot (c) and cells of the acute inflammatory infiltrate. (C) Orig. Mag. ×400. (D) Orig. Mag. ×1000. H-E Stain.

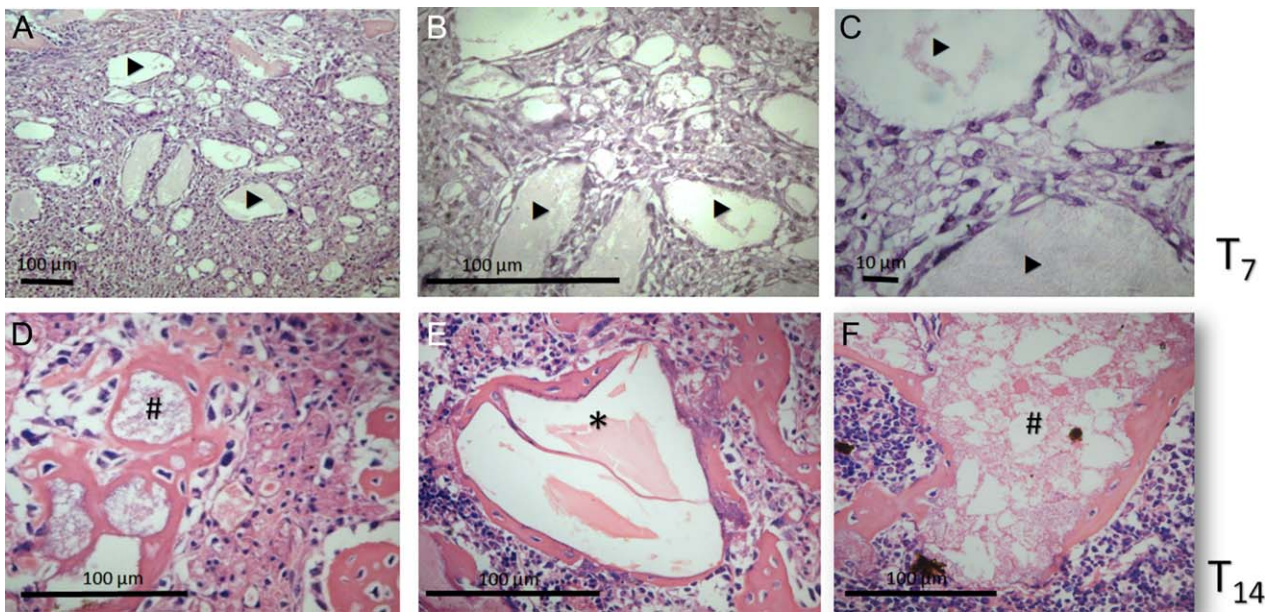

FIGURE 6. Histological study at T7 (A–C) and T14d (D–F). A–C show inorganic particles (▲) surrounded by reparative granulation tissue with abundant fibroblasts. A) Orig. Mag. ×100. (B) Orig. Mag. ×400 (C) Orig. Mag. ×1000. H–E Stain. (D–F) show inorganic particles surrounded by woven bone tissue at 14 days. (E) Note the presence of a BG (*) particle and D and F BC particles (#). D–F Orig. Mag. ×400 H-E Stain.

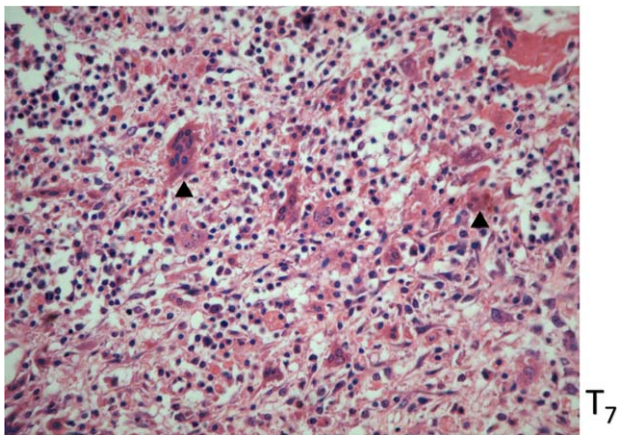

FIGURE 7. Histologic study at T7d. Abundant multinucleated giant cells (▶) can be seen at the center of the reparative granulation tissue. Orig. Mag. ×400. H-E Stain.

implantation.[47] The histologic findings observed in the present study at the initial time points, soon after implantation of the BCO in the rat tibia, confirmed this phenomenon.

There are reports on the use of collagen type I obtained from epidermal and bovine tendon or porcine tissue to make a matrix for BCO synthesis. This type of collagen is combined with BG[43,48–53] and calcium phosphates, such HA[27,34,35,54–59] and biphasic ceramics (HA plus β-TCP).[37–41,60,61]. The present study is the first to describe the novel use of WJ extracellular matrix as the organic phase of BCO providing a three-dimensional scaffold, which is a suitable platform for intercellular communication and biomaterial-cell interaction.

Despite the numerous research groups devoted to investigating stem cells obtained for tissue engineering applications, to our knowledge there are no reports in the literature on the use of WJ as a scaffold[44,46–48]

XRD and FTIR analysis revealed that BC particles were composed of β-TCP and HA, whereas the BG exhibited the characteristics of an amorphous material. Moreover, the average size of the inorganic particles was 282 ± 78 μm, as confirmed on SEM images. This size range is considered ideal for osteogenesis.[62]

The FTIR spectrum of BCO had frequencies for amide A, B, I, and II bands; the intensity of the peaks would seemingly depend on BC content. All collagen amides showed a red shift (to lower wave number) when BC was added to the WJ, suggesting collagen-BC interactions. As compared to the spectrum corresponding to WJ alone, the intensity of shifts of amides decreased as BC was added to the mixture, as follows: amide A decreased from 3468 to 3318 cm^{-1}, amide B from 2968 to 2930 cm^{-1}, whereas amide I shifted to a higher wave number from 1686 to 1656 cm^{-1}, amide II shifted from 1539 to 1537 cm^{-1}, and amide III disappeared. These results indicate that there is some degree of bonding between HA and collagen. The Ca^{+2} in the HA likely forms hydrogen bonds with the CONH and OH groups in the collagen. These bonds probably form with the proline and lysine in the collagen.[58,63]

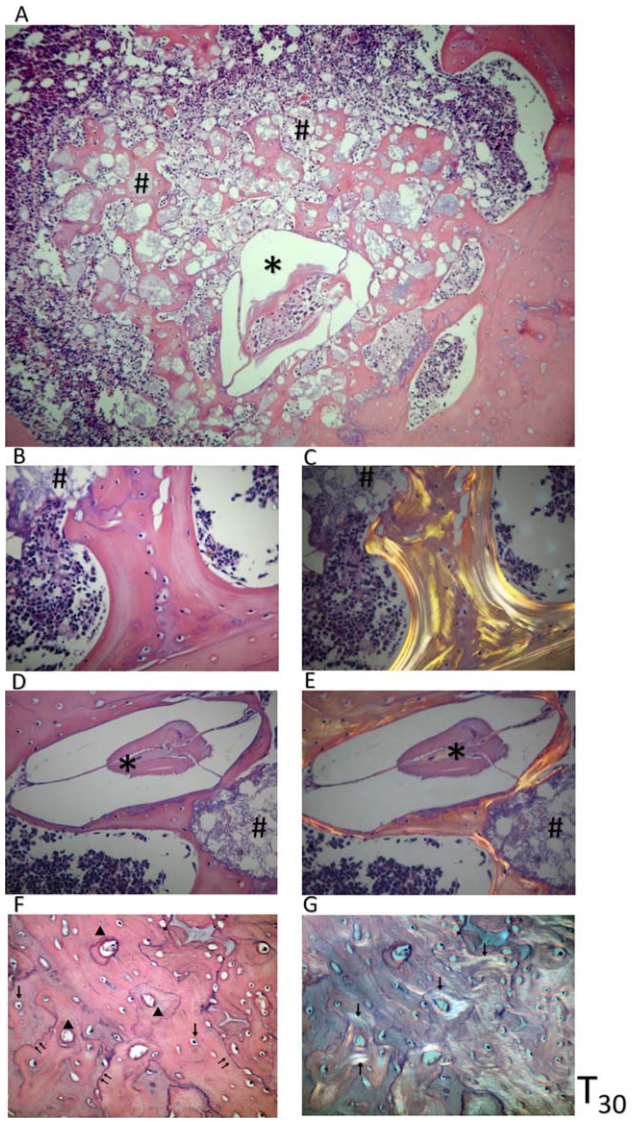

FIGURE 8. Histologic study at T30d. (A) Abundant BC particles (#) and a BG particle (*) are surrounded by lamellar bone. (B) Note the presence of lamellar bone and parallel alignment of collagen fibers, as seen using polarized light (C). (D) A BG particle (*) surrounded by lamellar bone, as seen using polarized light (E). AOrig. Mag. X100. B-E Orig. Mag. ×400. H-E Stain. (F) Bone tissue section showing the microstructure of lamellar bone. Note the presence of osteocytic lacunae containing osteocytes (→), Haversian-systems (▲), and a large number of incremental lines (↓↓). (G) Bone tissue section shown in microphotograph (F) as seen under polarized light. Note the parallel alignment of collagen fibers forming the lamellae of lamellar bone (↓). A) Orig. Mag. X100; B–G) Orig. Mag. ×400. H–E Stain.

The present work sought to develop a BCO with improved mechanical strengths for application in BTE in regions where the scaffolds are subjected to high levels of loading. A number of research groups have attempted to synthesize HA-collagen composites with adequate stiffness for clinical applications, but the obtained materials have shown poor mechanical properties.[9,10] This limited performance is a result of the procedure followed to obtain composite, precipitation of calcium phosphate on collagen fibers, since the process in itself does not ensure adequate bone architecture.

Mittlmier and Nizzard[64] were among the first researchers to attempt to develop a collagen–calcium phosphate composite, by mixing calcium phosphate granules with collagen web. Other researchers obtained these composites by mixing the calcium phosphate granules in a collagen suspension. Overall, the aforementioned composites showed a lack of cohesive strength, and were not entirely suitable for manufacturing implants that could be easily handled by surgeons and that had adequate biological properties.[27,34,35,55–59,64]

It is possible that the presence of fragments of hyaluronic acid (HAc) in WJ contributes to increasing the cohesion among the components of the biomaterial. The dry stage (previous to implantation) BCO WJ-BC-BG flexural strength was close to (40.3 ± 0.8) MPa and its flexural modulus was (2.44 ± 0.11) GPa, which is in the range of the best mechanical performance of calcium phosphate-collagen composites reported in the literature.[49,59] Nevertheless, these values are still far from the mechanical performance of healthy bone. Femoral bone has an ultimate flexural strength of (179.6 ± 19.4) MPa, and its flexural modulus is (10.8 ± 1.9) GPa (4.5-fold higher than that of the BCO presented here).

The best tensile strength magnitude reported to date is 96 MPa, and corresponds to a composite containing up to 5% (in wt) hyaluronic acid (HAc) (80HA-15Coll-5HAc). This value was found to decrease to 19 MPa when the HAc content of the composite was 0.8%.[47] It must be kept in mind, however, that these composites were obtained by compression moulding and heating at 200°C. It is likely that the collagen and HAc molecules became denatured at that temperature, thus affecting the biological response to the BCO. In addition, cross-linking collagen with glutaraldehyde in hot-pressed composites yields a bending strength of 21 MPa, as does a high HA content (up to 80% in wt.).[55] Crosslinking can be based on the formation of hydrogen bonds between collagen molecule chains and HA and β-TCP functional groups. This shows the importance of the molecular geometry as regards strength, toughness and energy dissipation properties.[63] In addition, it has been shown that there are complex crosslinks between calcium ions and the oxygen atoms in the proline amino acid.[58–63] The mechanical strength of BCO can be interpreted within the framework of qualitative and quantitative toughness studies of HA-collagen composites. A previous work reported mechanical strength of the composite to be higher than that of individual phases.[28] In addition, Young's modulus of pure HA was 3.6 GPa,[57] whereas incubation of HA in collagen solution increased the magnitude to 7.5 GPa. To assess the mechanical properties of a BCO, toughness of the HA-collagen composite itself must be assessed both qualitative and quantitatively, since the values obtained assessing each composite component separately are far lower than those observed when testing the composite. In line with studies reported in the literature, the compressive modulus of collagen scaffolds was found to increase 10-fold (from 20 to 200 KPa) when increasing HA particle content from 50% to 400% (in wt.).[63,64]

The biological response to this novel BCO was evaluated *in vivo*. The interaction between the surface of the biomaterial and the biological environment plays a fundamental role in the host's response. Our results showed that the BCO formed a hydrogel on its surface. Recent studies have demonstrated that matrices that generate hydrogels favor vasculogenesis.[65] In addition, a number of studies have shown that BG and BC promote neovessel formation both *in vitro* and *in vivo*, and are therefore suitable for application in bone tissue engineering.[66,67] Within the first 24 h post-implantation, the blood clot could be seen in close contact with the biomaterial, as well as acute inflammatory infiltrate surrounding the BC and BG particles. Our observation is in agreement with a study by Tapetyet al in deproteinized bone (Bio-OssTM), though the authors found this to occur 3 days post-implantation.[68] The healing process was enhanced by the ability of the hydrogel to absorb large amounts of liquid and provide a suitable platform for intercellular communication.[47] Seven days after implantation, granulation tissue and multinucleated giant cells (MNGCs) could be observed in some areas of the tissue. These cells were no longer observed 14 days post-implantation. In contrast with what was previously thought,[69] it is well documented at present that MNGCs stimulate vasculogenesis and angiogenesis through the release of different chemical mediators, such as vascular endothelial growth factor (VEGF).[70,71] In their study on biological response to small Bio-OssTM particles, Barbecket al. detected MNGCs between days 10 and 15 post-implantation, and found the number of these cells to decrease toward 30 days post-placement, with only few remaining at 60 days.[70,71] The finding of MNGCs does not necessarily imply a negative response of the host to the biomaterial, and must be evaluated in terms of the persistence of these cells through time, since their presence can have a positive effect on vascularization and the healing process.

No inflammatory infiltrate and no MNGCs were observed 14 days post-implantation, and woven bone was found amalgamating the BG and BC particles. The high biocompatibility of the inorganic components (BG and BC) is well documented.[2–8,12–16] Hench et al showed the ability of BG to form HA on its surface and promote differentiation of undifferentiated mesenchymal cells into osteoblasts.[12–16] Polak et al. demonstrated the ability of BG to stimulate seven specific genes to increase the population of osteoblasts at the biomaterial implantation site, as a result of the release of ionic products.[15] As regards BC, in addition to being osteoconductive, biphasic BC (HA + β-TCP) also promotes osteogenesis, and its degradation rate matches the growth rate of the target tissue.[2,3,6,12,13]

A number of authors have used stem cells derived from the umbilical cord, and have highlighted their osteogenic potential. Nevertheless, there are no reports on the use of WJ as a matrix for BCO.[44,46,48] WJ is a reservoir of growth factors and mainly consists of collagen, hyaluronic acid, and sulfated glycosaminoglycans (GAGs). The latter play an important role in cell–cell and cell–extracellular matrix interactions. Rodrigues et al. found that the collagen (COL) in a HA-COL composite provides binding sites for growth

factors, and improves the mechanical properties of the biomaterial.[72]

Thirty days post-implantation, the woven bone had been replaced with lamellar bone, which can satisfactorily meet its mechanical demands.[57] All the aforementioned findings show the high biocompatibility and osteogenic capacity of the new biomaterial proposed herein.

CONCLUSIONS

A novel biocomposite (BCO) was synthesized and characterized. The biocomposite is based on the combination of Wharton's jelly (WJ), as the organic matrix, and inorganic bioceramic (BC) and bioactive glass (BG) particles. The synthesized composite, which has not been described in the literature to date, showed high toughness and was suitable for tissue regeneration and lamellar bone formation. The newly formed lamellar bone was found to form bridges amalgamating the inorganic particles, which is of utmost importance from the biomechanical point of view. The physical–chemical properties of BCO and the observed biological response to this biocomposite render it suitable for clinical applications.

ACKNOWLEDGMENTS

The authors specially thank Dr Sandra Renou for her assistance in editing the photographs.

REFERENCES

1. MacDuff E, Reid R. Bone tumour pathology. Surgery 2009;27:55–62.
2. Salgado AJ, Coutinho OP, Reis RL. Bone tissue engineering: State of the art and future trends. Macromol Biosci 2004;4:743–765.
3. Hutmacher DW. Scaffolds in tissue engineering bone and cartilage. Biomaterials 2000;21:2529–2543.
4. Petite H, Viateau V, Bensaïd W, Meunier A, De Pollak C, Bourguignon M, Oudina K, Sedel, Guillemin L. Tissue-engineered bone regeneration. Nat Biotechnol 2000;18:959–963.
5. Klein P, Schell H, Streitparth F, Heller M, Kassi J, Kandziora F, Bragulla H, Haas NP, Duda GN. The initial phase of fracture healing is specifically sensitive to mechanical conditions. J Orthop Res 2003;21:662–669.
6. Shin H, Mikos AG. Biomimetic materials for tissue engineering. Biomaterials 2003;24:4353–4364.
7. Henkel K, Gerber T, Dörfling P, Gundlach K, Bienengräber V. Repair of bone defects by applying biomatrices with and without autologous osteoblasts. J Craniomaxillofac Surg 2005;33:45–49.
8. Kim H, Jung G, Yoon J, Han J, Park Y, Kim D, Zhang M, Kim D. Preparation and characterization of nano-sized hydroxyapatite/alginate/chitosan composite scaffolds for bone tissue engineering. Mat Sci and Eng C 2015;54:20–25.
9. Quinlan E, Thompson E, Matsiko A, O'Brien F, López-Noriega A. Long-term controlled delivery of rhBMP-2 from collagen–hydroxyapatite scaffolds for superior bone tissue regeneration. J Control Release 2015;207:112–119.
10. Schneider R, Puellen A, Kramann R, Raupach K, Bornemann J, Knuechel R, Pérez-Bouza A, Neuss S. The osteogenic differentiation of adult bone marrow and perinatal umbilical mesenchymal stem cells and matrix remodelling in three-dimensional collagen scaffolds. Biomaterials 2010;31:467–480.
11. Carlton A, Holmes RE. Hydroxyapatite and tricalcium phosphate bone graft substitutes. Orthop Clin North Am 1987;18:323–334.
12. Hench LL. Ceramics, glasses and glass-ceramics. In: Ratner BD, Hoffman AS, Lemons JE, editors. Biomaterials Science: An Introduction to Materials in Medicine, 2nd ed. San Diego, CA: Elsevier Academic Press; 2004. p 73–84.
13. Hench LL. Bioceramics. J Am Ceram Soc 1998;81:1705–1727.
14. Cao W, Hench LL. Bioactive materials. Ceram Int 1996;22:493–507.
15. Hench LL, Polak JM. Third-generation biomedical materials. Science 2002;295:1014–1017.
16. Hench LL. The story of bioglass®. J Mater Sci Mater Med 2006;17:967–978.
17. Aniket RR, Hall B, Marriott I, El-Ghannam A. Early osteoblast responses to orthopedic implants: Synergy of surface roughness and chemistry of bioactive ceramic coating. J Biomed Mater Res A 2015;103:1961–1973.
18. El-Ghannam A, Ning CQ. Effect of bioactive ceramic dissolution on the mechanism of bone mineralization and guided tissue growth *in vitro*. J Biomed Mater Res A 2006;76:386–397.
19. El-Ghannam A. Advanced bioceramic composite for bone tissue engineering: Design principles and structure-bioactivity relationship. J Biomed Mater Res A 2004;69:490–501.
20. Aniket YA, Marriott I, El-Ghannam A. Promotion of pro-osteogenic responses by a bioactive ceramic coating. J Biomed Mater Res A 2012;100:3314–3325.
21. Salma-Ancane K, Stipniece L, Putnins A, Berzina-Cimdina L. Development of Mg-containing porous β-tricalcium phosphate scaffolds for bone repair. Ceram Int 2015;41:4996–5004.
22. Cabrini RL, Guglielmotti MB, Almagro JC. Histomorphometry of initial bone healing around zirconium implants in rats. Implant Dent 1993;2:264–267.
23. Plewinski M, Schickle K, Lindner L, Kirsten A, Weber M, Fische H. The effect of crystallization of bioactive bioglass 45S5 on apatite formation and degradation. Dent Mater 2013;29:1256–1264.
24. Letaief N, Lucas-Girot A, Oudadesse H, Meleard P, Pott T, Jelassi J, Dorbez-Sridi R. Effect of aging temperature on the structure, pore morphology and bioactivity of new sol–gel synthesized bioglass. J Non Cryst Solids 2014;402:194–199.
25. Guo X, Yan H, Zhao S, Zhang L, Li Y, Liang X. Effect of calcining temperature on particle size of hydroxyapatite synthesized by solid-state reaction at room temperature. Adv Powder Technol 2013;24:1034–1038.
26. Sha L, Liu Y, Zhang Q, Hu M, Jiang Y. Microwave-assisted coprecipitation synthesis of high purity β-tricalcium phosphate crystalline powders. Mater Chem Phys 2011;129:1138–1141.
27. Bakhtiari L, Rezaie HR, Hosseinalipour SM, Shokrgozar MA. Investigation of biphasic calcium phosphate/gelatin nanocomposite scaffolds as a bone tissue engineering. Ceram Int 2010;36:2421–2426.
28. Scalera F, Gervaso F, Sanosh P, Sannino A, Licciulli A. Influence of the calcination temperature on morphological and mechanical properties of highly porous hydroxyapatite scaffolds. Ceram Int 2013;39:4839–4846.
29. Lee DS, Pai Y, Chang S. Effect of pH control of mixture solution on the fabrication of the highly pure β-tricalcium phosphate powders synthesized by liquid–solid mixture precipitation method. Mater Lett 2013;102:76–79.
30. Qian J, Kang Y, Wei Z, Zhang W. Fabrication and characterization of biomorphic 45S5 bioglass scaffold from sugarcane. Mater Sci and Eng C 2009;29:1361–1364.
31. Ma J, Chen CZ, Wang DG, Meng XG, Shi JZ. Influence of the sintering temperature on the structural feature and bioactivity of sol–gel derived SiO_2–CaO–P_2O_5 bioglass. Ceram Int 2010;36:1911–1916.
32. Twardowski J, Anzenbacher P. Raman and IR Spectroscopy in Biology and Biochemistry. Chichester, UK: Ellis Horwood Ltd; 1994.
33. Singh BR. Infrared Analysis of Peptides and Proteins: Principles and Applications. Corby, UK: Amer Chem Soc Series 750, Oxford Univ. Press; 2000.
34. Chang MC, Ko C, Douglas WH. Conformational change of hydroxyapatite/gelatin nanocomposite by glutaraldehyde. Biomaterials 2013;24:3087–3094.
35. Camacho NP, West P, Torzilli PA, Mendelsohn R. FTIR microscopic imaging of collagen and proteoglycan in bovine cartilage. Biopolymers 2011;62:1–8.
36. Meng Z, Zheng X, Tang K, Liu J, Ma Z, Zhao Q. Dissolution and regeneration of collagen fibers using ionic liquid. Int J Biol Macromol 2012;51:440–448.

37. Santos MH, Dias Heneine LG, Sander Mansur H. Synthesis and characterization of calcium phosphate/collagen biocomposites doped with Zn^{2+}. Mat Sci Eng C 2008;28:563–571.
38. Boryskina OP, Bolbukh TV, Semenov MA, Gasan AI, Maleev V. Energies of peptide–peptide and peptide–water hydrogen bonds in collagen: Evidences from infrared spectroscopy, quartz piezogravimetry and differential scanning calorimetry. J Mol Struct 2007;827:1–10.
39. Fan Y, Duan K, Wang R. A composite coating by electrolysis-induced collagen self-assembly and calcium phosphate mineralization. Biomaterials 2005;26:1623–1632.
40. Xu Z, Neoh KG, Kishen A. A biomimetic strategy to form calcium phosphate crystals on type I collagen substrate. Mat Sci Eng C 2010;30:822–826.
41. Vidal B, Mello ML. Collagen type I amide I band infrared spectroscopy. Micron 2011;42:283–289.
42. Kandamchira A, Selvam S, Marimuthu N, Janardhanan SK, Fathima NN. Influence of functionalized nanoparticles on conformational stability of type I collagen for possible biomedical applications. Mater Sci Eng C 2013;33:4985–4988.
43. Roveri N, Falini G, Sidoti MC, Tampieri A, Landi E, Sandri M, Parma B. Biologically inspired growth of hydroxyapatite nanocrystals inside self-assembled collagen fibers. Mater Sci Eng C 2003;23:441–446.
44. Sobolewski K, Małkowski A, Bańkowski E, Jaworski S. Wharton's jelly as a reservoir of peptide growth factors. Placenta 2005;26: 747–752.
45. Dhimolea E, Maffini MV, Soto AM, Sonnenschein C. The role of collagen reorganization on mammary epithelial morphogenesis in a 3D culture model. Biomaterials 2010;31:3622–3630. Volume Issue Pages
46. Taghizadeh RR, Cetrulo KJ, Cetrulo CL. Wharton's jelly stem cells: Future clinical applications. Placenta 2011;32:11–15.
47. Kisiel M, Martino M, Ventura M, Hubbell J, Hilborn J, Ossipov D. Improving the osteogenic potential of BMP-2 with hyaluronic acid hydrogel modified with integrin-specific fibronectin fragment. Biomaterials 2013;34:704–712.
48. Fong CY, Subramanian A, Biswas A, Gauthaman K, Srikanth P, Bongso A. Derivation efficiency, cell proliferation, freeze–thaw survival, stem-cell properties and differentiation of human Wharton's jelly stem cells. Rep BioMed 2010;21:331–340.
49. Lin X, Li X, Fan H, Wen X, Lu J, Zhang J. In situ synthesis of bone-like apatite/collagen nano-composite at low temperature. Mater Lett 2004;58:3569–3572.
50. Herten SM, Ferrari D, Wieland M, Schmitz L, Engelhardt E, Becker J. Guided bone regeneration at dehiscence-type defects using biphasic hydroxyapatite + beta tricalcium phosphate (Bone Ceramic) or a collagen-coated natural bone mineral (BioOss Collagen): An immunohistochemical study in dog. Int J Oral Maxillofac Surg 2007;36:1198–1206.
51. Leu JK. Proangiogenic potential of a collagen/bioactive glass substrate. Pharm Res 2008;25:1222–1229.
52. Pek YS, Gao S, Arshad MS, Leck K, Ying JY. Porous collagen-apatite nanocomposite foams as bone regeneration scaffolds. Biomaterials 2008;29:4300–4305.
53. Heinemann S, Heinemann C, Bernhardt R, Reinstorf A, Nies B, Meyer M, Worch H, Hanke T. Bioactive silica–collagen composite xerogels modified by calcium phosphate phases with adjustable mechanical properties for bone replacement. Acta Biomater 2009; 5:1979–1990.
54. Desimone MF, Hélary C, Rietveld I, Bataille I, Mosser G, Giraud-Guille M, Livage J, Coradin T. Silica–collagen bionanocomposites as three-dimensional scaffolds for fibroblast immobilization. Acta Biomater 2010;6:3998–4004.
55. Kikuchi M, Ikoma T, Itoh S, Matsumoto HN, Koyama Y, Akakuda K, Shinomiya K, Tanaka J. Biomimetic synthesis of bone-like nanocomposites using the self-organization mechanism of hydroxyapatite and collagen. Compos Sci Technol 2004;64:819–825.
56. Li J, Chen Y, Mak AF, Tuan R, Li L, Li Y. A one-step method to fabricate PLLA scaffolds with deposition of bioactive hydroxyapatite and collagen using ice-based microporogens. Acta Biomater 2010;6:2013–2019.
57. Katti DR, Pradhan SM, Katti KS. Directional dependence of hydroxyapatite-collagen interactions on mechanics of collagen. J Biomech 2010;43:1723–1730.
58. Sionkowska A, Kozłowsk J. Characterization of collagen/hydroxyapatite composite sponges as a potential bone substitute. Int J Biol Macromol 2010;47:483–487.
59. Zhang L, Tang P, Xu M, Zhang W, Chai W, Wang Y. Effects of crystalline phase on the biological properties of collagen–hydroxyapatite composites. Acta Biomater 2010;6:2189–2199.
60. Tamimi F, Kumarasami B, Doillon C, Gbureck U, Le Nihouannen D, Lopez Cabarcos E, et al. Brushite–collagen composites for bone regeneration. Acta Biomater 2008;13:1315–1321.
61. Li L, Lin Z, Zheng Q, Guo X, Lan S, Liu S, Yang S. Repair of rabbit radial bone defects using true bone ceramics combined with BMP-2-related peptide and type I collagen. Mater Sci Eng: C 2010; 30:1272–1279.
62. Oonishi H, Hench LL, Wilson J, Sugihara F, Tsuji E, Kushitani S, Iwaki S. Comparative bone growth behaviour in granules of bioceramic materials of different particle sizes. J Biomed Mater Res A 1999;44:31–43.
63. Libonati F, Nair AK, Vergani L, Buehler MJ. Mechanics of collagen–hydroxyapatite model nanocomposites. Mech Res Commun 2014;58:17–23.
64. Liu A. Collagen–hydroxyapatite composite scaffolds for tissue engineering: Woodhead Publishing Series in Biomaterials. Cambridge, UK: Woodhead Publishing; 2015. 211–234.
65. Hanjaya-Putra D, Wong KT, Hirotsu K, Khetan S, Burdick J, Gerecht S. Spatial control of cell-mediated degradation to regulate vasculogenesis and angiogenesis in hyaluronan hydrogels. Biomaterials 2012;33:6123–6131.
66. Quinlan E, Partap S, Azevedo M, Jell G, Stevens M, O'Brien F. Hypoxia-mimicking bioactive glass/collagen glycosaminoglycan composite scaffolds to enhance angiogenesis and bone repair. Biomaterials 2015;52:358–366.
67. Li H, Chang J. Stimulation of proangiogenesis by calcium silicate bioactive ceramic. Acta Biomater 2013;9:5379–5389.
68. Tapety FI, Amizuka N, Uoshima K, Nomura S, Maeda T. A histological evaluation of the involvement of Bio-Oss in osteoblastic differentiation and matrix synthesis. Clin Oral Implants Res 2004; 15:315–324.
69. Franz S, Rammelt S, Scharnweber D, Simon JC. Immune responses to implants. A review of the implications for the design of immunomodulatory biomaterials. Biomaterials 2011;32:6692–6709.
70. Barbeck M, Udeabor SE, Lorenz J, Kubesch J, Choukroun J, Sader RA, Kirkpatrick CJ, Ghanaati S. Induction of multinucleated giant cells in response to small sized bovine bone substitute (Bio-Oss TM) results in an enhanced early implantation bed vascularization. Ann Maxillofac Surg 2014;4:150–157.
71. Ghanaati S, Unger R, Webber MJ, Barbeck M, Orth C, Kirkpatrick JA, Booms P, Motta A, Migliaresi C, Sader R, Kirkpatrick C. Scaffold vascularization *in vivo* driven by primary human osteoblasts in concert with host inflammatory cells. Biomaterials 2011;32: 8150–8160.
72. Rodrigues CV, Serricella P, Linhares AB, Guerdes RM, Borojevic R, Rossi MA, Duarte ME, Farina M. Characterization of a bovine collagen–hydroxyapatite composite scaffold for bone tissue engineering. Biomaterials 2003;24:4987–4997.